Multilayer Perceptron-Based Volt/Var Droop Control with Harmonic Impact Analysis

Wonyoung Choi
School of Electrical and Electronic Engineering
Inha University
Incheon, South Korea
wonyoung@inha.ac.kr

Insu Kim
School of Electrical and Electronic Engineering
Inha University
Incheon, South Korea
insu@inha.ac.kr

***Abstract*—This paper proposes a Volt/Var control strategy based on a multilayer perceptron (MLP) to improve the voltage regulation capability of photovoltaic (PV) inverters under time-varying load and generation conditions. The proposed model is trained to capture the nonlinear droop characteristics between voltage and the reactive power reference (Q_{ref}^{*}) using data generated from dynamic droop simulations. The MLP is trained with 57,600 samples using the Levenberg-Marquardt algorithm and demonstrates excellent regression performance (R=0.997). The case study evaluates three operating modes over a 24-hour period. Results show that the MLP-based control achieves nearly identical voltage regulation to the conventional droop method, with minimal deviation (MSE=7.27×10^{-7}, MAE=5.14×10^{-4}). Furthermore, harmonic analysis based on the Q_{ref}^{*} indicates that the proposed approach maintains consistent harmonic voltage and THD levels compared to the conventional droop method. These findings demonstrate that the MLP-based Volt/Var control effectively replicates traditional control performance while providing superior adaptability and learning capability under uncertain grid conditions. The proposed method shows potential for real-time adaptive voltage regulation in distribution networks with high renewable penetration.**

***Keywords*—multilayer perceptron (MLP), Volt/Var control, reactive power prediction, photovoltaic (PV) inverter, voltage regulation, harmonic analysis.**

I. Introduction

The increasing penetration of distributed energy resources (DERs), such as photovoltaic (PV) and wind power, has significantly affected grid voltage regulation [1, 2]. Therefore, maintaining voltage stability in modern power networks has become a critical concern. One of the most effective strategies for voltage regulation is Volt/Var control method, which adjusts reactive power absorption or injection at buses where the voltage magnitude deviates from the acceptable range [3, 4]. Consequently, Volt/Var control has become essential for mitigating voltage fluctuations caused by the growing integration of DERs. However, most existing studies on Volt/Var control have primarily focused on voltage stability improvement, while the impact of reactive power control on harmonic distortion has received limited attention. To address this limitation, this study analyzes the harmonic effects resulting from reactive power exchange through Volt/Var control.

Recently, artificial intelligence (AI) techniques have gained considerable attention in power system operation for modeling nonlinear mappings and enhancing control adaptability. Typical approaches include multilayer perceptrons (MLP), convolutional neural networks (CNN), long short-term memory (LSTM) networks, and reinforcement learning algorithms [5-8]. In this work, an MLP-based Volt/Var control framework is proposed to enhance voltage regulation under time-varying PV and load conditions. Unlike conventional droop-based Volt/Var control, which relies on iterative computation and often suffers from time delays, the proposed MLP model efficiently learns the nonlinear relationship between bus voltage and reactive power reference (Q_{ref}^{*}), enabling fast and adaptive control. Furthermore, by applying the Q_{ref}^{*} to the harmonic analysis, the proposed approach evaluates the harmonic impacts accurately. The main contributions of this study are summarized as follows:

Accurate Q_{ref}^{*} prediction using MLP. The proposed MLP model effectively learns the nonlinear Volt/Var droop characteristic, providing accurate prediction of the Q_{ref}^{*} under time-varying PV and load conditions.

Harmonic analysis based on predicted Q_{ref}^{*}. The harmonic voltages and total harmonic distortion (THD) computed using the MLP-predicted Q_{ref}^{*} show close agreement with those obtained from conventional droop control, confirming the precision of the proposed method.

Regression-based Q_{ref}^{*} estimation as a lightweight surrogate. A polynomial regression model derived from MLP-generated dataset provides an additional lightweight surrogate for Q_{ref}^{*} estimation. It enables simplified and computationally efficient Q_{ref}^{*} prediction.

II. Proposed Methods

A. Overview

Conventional Volt/var control adjusts Q_{ref}^{*} based on the deviation of the bus voltage (V_{bus}) from a reference value (V_{ref}).

This research was supported by the 2026 Energy Human Resource Development Program (Center for AI-Converged Microgrid-based Next-Generation Power Grid Workforce Development of Inha University) of the Korea Institute of Energy Technology Evaluation and Planning, funded by the Ministry of Climate, Energy and Environment, Republic of Korea.

979-8-3315-8138-1

As shown in Fig. 1, when the voltage decreases below the lower voltage limit (V_{deadL}), the inverter injects reactive power to support the voltage.

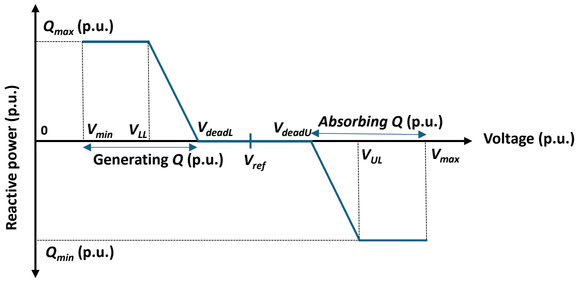

Fig. 1. Volt/Var droop curve.

Conversely, when the voltage exceeds the upper voltage limit (V_{deadU}), the inverter absorbs reactive power to suppress overvoltage. Within the deadband region ($V_{deadL} \leq V_{ref} \leq V_{deadU}$), no reactive power is exchanged. This behavior can be expressed as shown in (1).

$$Q^*(V) = \begin{cases} Q_{\max}, \quad V \leq V_{LL} \\ Q_{\max} + \dfrac{0 - Q_{\max}}{V_{deadL} - V_{LL}}(V - V_{LL}), \quad V_{LL} < V < V_{deadL} \\ 0, \quad V_{deadL} \leq V \leq V_{deadU} \\ \dfrac{Q_{\min} - 0}{V_{UL} - V_{deadU}}(V - V_{deadU}), \quad V_{deadU} < V < V_{UL} \\ Q_{\min}, \quad V \geq V_{UL} \end{cases} \tag{1}$$

where Q_{max} and Q_{min} are the upper and lower reactive power limits of the inverter, respectively.

In this study, the droop parameters (V_{min}, V_{LL}, V_{deadL}, V_{deadU}, V_{UL}, V_{max}, Q_{max}, Q_{min}) are randomly varied within predefined ranges as summarized in Table 1, and the MLP-based model is trained to predict the Q_{ref}^* corresponding to each combination. This approach enables the AI model to learn the nonlinear relationship among system variables such as inverter bus voltage, PV output power, and local load.

B. Data Generation for MLP Training

To train the MLP for adaptive Volt/Var control, a large set of training data was generated through time-domain simulations of the power system under various droop parameter settings. Each simulation represents a 24-hour operation of the power system with a PV inverter installed at the distribution bus. At every 5-minute interval ($T = 288$ steps), the active power of the PV source (P_{pv}) and the system load (P_{load}, Q_{load}) were updated based on realistic daily profiles in p.u. The bus voltage magnitude was computed using the Newton-Raphson power flow analysis. Based on the selected droop parameters, the corresponding $Q_{ref}^*(V)$ is obtained from (1). The reactive power capacity (Q_{cap}) was defined as follows.

$$Q_{cap} = \sqrt{S_r^2 - P_{PV}^2} \quad \text{(in p.u.)} \tag{2}$$

where S_r denotes the inverter's rate apparent power in p.u.

The parameter variation ranges are summarized in Table 1.

Table 1. Parameter ranges for dynamic data generation

Parameter	Range / Description
V_{min}	[0.92p.u., 0.96p.u.]
V_{LL}	$V_{min} + \Delta$, where $\Delta \in$ [0.01p.u., 0.03p.u.]
V_{deadL}	[0.990p.u., 0.995p.u.]
V_{deadU}	[1.005p.u., 1.010p.u.]
V_{UL}	$V_{deadU} + \Delta$, where $\Delta \in$ [0.02p.u., 0.05p.u.], $V_{UL} \leq$ 1.06p.u.
V_{max}	$V_{UL} + \Delta$, where $\Delta \in$ [0.01p.u., 0.03p.u.], $V_{max} \leq$ 1.10p.u.
RN_{up}	Random scaling factor for Q_{max}, $RN_{up} \in$ [0.8, 1.0]
RN_{dn}	Random scaling factor for Q_{min}, $RN_{dn} \in$ [0.3, 0.6]
Q_{max}	$RN_{up}Q_{cap}$ (in p.u.)
Q_{min}	$- RN_{dn}Q_{cap}$ (in p.u.)
P_{PV}	Gaussian daily irradiance profile [0.0p.u., 1.0p.u.]
P_{load}, Q_{load}	Scaled by 24-hour base load ratio (in p.u.), power factor = 0.95

At each time step k, the MLP input vector ($X(k)$) and output label ($y(k)$) were defined as:

$$\begin{aligned} X(k) &= \left[V_{bus}(k), P_{PV}(k), P_{load}(k), Q_{load}(k), V_{\min}, V_{LL}, V_{deadL}, V_{deadU}, V_{UL}, V_{\max}, RN_{up}, RN_{dn}, Q_{prev}(k)\right]^{\mathrm{T}} \\ y(k) &= Q_{ref}^*(k) \end{aligned} \tag{3}$$

Here, droop parameters are explicitly included as part of the input features, allowing the network to learn how these parameters affect the reactive power response. The bus voltage ($V_{bus}(k)$) is determined by the previously applied reactive power command ($Q_{prev}(k)$) and the present load condition. The sinusoidal time embedding terms help the model capture the daily cyclical pattern of PV generation and load variation. By iterating over multiple random combinations of the droop parameters listed in Table 1, a comprehensive dataset was obtained that covers both under- and over voltage operating conditions. This dataset enables the MLP to infer an optimal Q_{ref}^* command for any arbitrary combination of V_{bus}, P_{pv}, and droop parameters.

C. MLP Model Structure and Training Process

The proposed adaptive Volt/Var controller employs an MLP implemented using MATLAB's *fitnet* function. The MLP learns the nonlinear mapping between the input feature vector ($X(k)$) and the corresponding $Q^*(k)$. The training inputs explicitly include droop parameters so that the network can capture how droop parameters influence the reactive power response under different operating conditions. Table 2 summarizes the core configuration of the proposed MLP used for adaptive Volt/Var control.

Table 2. Configuration of the proposed MLP for Volt/Var control

Component	Description
Input layer	13 neurons [V_{bus}, P_{PV}, P_{load}, Q_{load}, V_{min}, V_{LL}, V_{deadL}, V_{deadU}, V_{UL}, V_{max}, η_{up}, η_{dn}, Q_{prev}]
Hidden layers	2 layers, 20 neurons each (*tansig* activation in MATLAB)
Output layer	1 neuron: Q_{ref}^*
Training algorithm	Levenberg-Marquardt (*trainlm* in MATLAB)
Data split	70% training, 15% validation, and 15% testing.

The network consists of two hidden layers with *tansig* activation and one output neuron predicting the Q_{ref}^*. The Levenberg-Marquardt algorithm (*trainlm*) was employed for efficient convergence, with the dataset divided into training, validation, and testing in a 70:15:15 ratio. The forward mapping of the proposed MLP is defined as (4).

$$Q_{MLP}^* = f_\theta(X) = W_3\phi_2(W_2\phi_1(W_1X + b_1) + b_2) + b_3 \tag{4}$$

where W_1, W_2, W_3 are the weight matrices, b_1, b_2, b_3 are the bias vectors, and ϕ_1, ϕ_2 denote the activation function used in

979-8-3315-8138-1

each hidden layer. The parameter set ($\theta = W_1, W_2, W_3, b_1, b_2, b_3$) is optimized through supervised learning to minimize the mean-squared-error (MSE) objective as follows.

$$J(\theta) = \frac{1}{N}\sum_{k=1}^{N}(Q^*(k) - Q^*_{MLP}(k))^2 \tag{5}$$

The $Q^*(k)$ used for training is obtained from droop-based control simulations performed under diverse droop parameters. The dataset covers 24-hour operation with 5-minite intervals, capturing variations in PV output, load, and voltage. After convergence, the MLP effectively generalizes to unseen operating conditions and replaces the conventional droop function by generating the instantaneous Q^*_{MLP}.

D. Harmonic Voltage and Total Harmonic Distortion Computation Using MLP-Based Reactuve Power Command

After obtaining the Q^*_{MLP} from the trained network, the inverter at the PV bus injects a complex power (S_{PV}) composed of both active and reactive components as:

$$S_{PV} = P_{PV} + jQ^*_{MLP} \quad \text{(in p.u.)} \tag{6}$$

The corresponding fundamental current injected by the PV inverter is obtained as follows.

$$I_{fund} = \left(\frac{S_{PV}}{V_{fund}}\right)^* \quad \text{(in p.u.)} \tag{7}$$

where V_{fund} is the fundamental voltage at the inverter bus.

The harmonic current components injected from DG are determined as a percentage of the fundamental current is formulated as formulated in (8).

$$I_h = \alpha_h \cdot I_{fund} \quad \text{(in p.u.)} \tag{8}$$

where α_h represents the harmonic current ratio for the h-th order.

Using the harmonic-impedance matrix (Z_h) constructed for each harmonic order, the harmonic voltage at each bus can be computed using (9).

$$\begin{aligned} V_h &= Z_h \cdot I_{h,final} \quad \text{(in p.u.)} \\ V_h &= Z_h \cdot I_{h,final} \cdot 100 \quad \text{(in \%)} \end{aligned} \tag{9}$$

Here, each Z_h is derived from the lines and generators and $I_{h,\,final}$ represents the vector of harmonic currents injected into or drawn from each bus at the h-th order.

The THD of voltage is computed as follows:

$$THD_V = \frac{\sqrt{\sum_{h=2}^{50}|V_h|^2}}{|V_{fund}|} \times 100\% \tag{10}$$

Finally, the calculated V_h and THD_V are verified for compliance with the IEEE Standards 519 [9].

III. Case Studies

To validate the proposed MLP-based Volt/Var control strategy and evaluate its effectiveness under various operating conditions, this section presents multiple case studies. The test system is used as the benchmark network [10]. PV generation is added to the system, and the load demand is varied over a 24-hour period to simulate dynamic operating conditions. The inverter's Q_{ref}^* is determined by the trained MLP model, and for comparison purposes, both the conventional droop control and the proposed MLP-based control are applied under identical conditions.

A. Verification of MLP Training Performance

To verify the learning capability and accuracy of the proposed MLP model, the training process was conducted using 57,600 samples generated from 200 randomized droop parameters over 24 hours. The network structure consisted of two-hidden layers with ten neurons each, and the training was performed using the Levenberg-Marquardt (*trainlm*) algorithm in MATLAB. The dataset was divided into 70% for training, 15% for validation, and 15% for testing. As shown in Fig. 2, the MLP model converged with a minimum validation MSE of 5.97×10^{-4} at epoch 218.

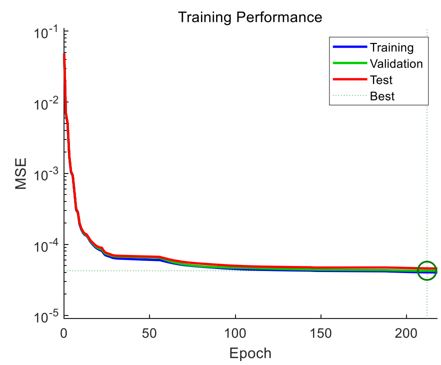

Fig. 2. Training performance of the proposed MLP model, showing the evolution of MSE for training, validation, and testing datasets.

The regression results of the proposed MLP model are illustrated in Fig. 3. Each subplot represents the correlation between the predicted and target reactive power values for training, validation, testing, and all datasets.

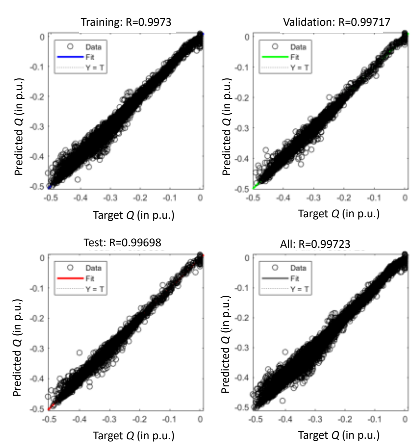

Fig. 3. Regression performance of the trained MLP model for training, validation, testing, and all datasets.

As shown in the figure, all regression plots exhibit a strong linear relationship with correlation coefficients (R) exceeding 0.997, indicating that the proposed MLP

979-8-3315-8138-1

successfully captures the nonlinear mapping between input features and predicted Q.

The trained MLP model is approximated by a second-order regression surrogate to express the nonlinear relationship. The regression form can be expressed as shown in (11).

$$Q^{*} = c_0 + \sum_{i=1}^{n}\left(a_i x_i + b_i x_i^2\right) \tag{11}$$

where x_i represents the i-th input feature, n is the total number of input variables, a_i and b_i denote the linear and quadratic coefficients, respectively, and c_0 is a constant term. The complete set of regression coefficients is provided in Appendix A.

B. Comparison Among Conventional Droop, MLP-Based Control, and Regression Model

To assess the effectiveness of the proposed MLP-based Q_{ref}^{*} control, a time-series simulation was carried out over a 24-hour period using PV and load profiles at bus 9. In this evaluation, three control strategies were tested and compared. Fig. 4 compares the Q_{ref}^{*} generated by the conventional droop and the MLP-based controller, and the regression-based model over a 24-hour period.

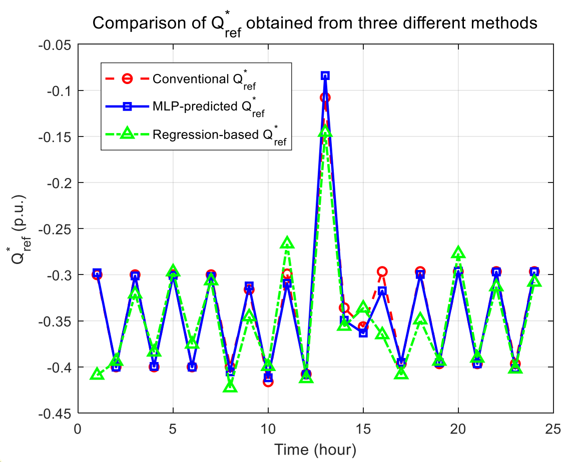

Fig. 4. Comparison of Q_{ref}* between conventional droop control and MLP prediction over 24 hours.

The three Q_{ref}^{*} profiles show nearly identical trends over the 24-hour period. The MLP prediction closely matches the conventional droop response across all hours, confirming that it accurately captures the underlying Volt/Var characteristic. Although the regression model exhibits a larger deviation at the first time step, it aligns well with the other two methods thereafter. Between 12:00 and 14:00, when PV generation sharply increases, both the MLP and regression models predicted Q_{ref}^{*} closely follows the conventional droop response. Fig. 5 shows the comparison of bus voltage under three different control modes.

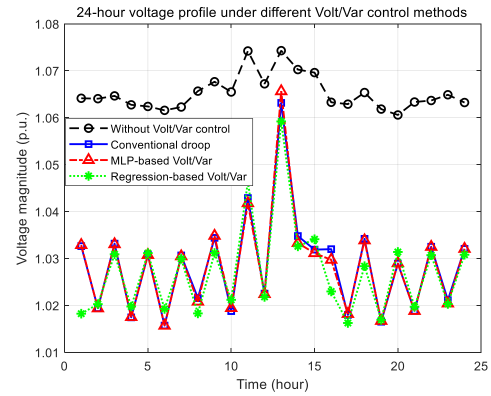

Fig. 5. 24-hour voltage profiles under four different control methods.

Without droop control, the voltage remains above 1.06 p.u., indicating sustained overvoltage conditions. When conventional droop control is applied, the inverter absorbs reactive power and the voltage effectively regulated. The MLP-based controller produces a voltage profile that is nearly identical to the conventional droop result, confirming that it successfully learns and reproduces the underlying Volt/Var behavior. The regression-based model also follows a similar trend, with small deviations at certain time steps, particularly at the initial hour, due to its simplified polynomial structure.

C. Harmonic Analysis Based on MLP-Predicted Reactive Power

This section presents the harmonic analysis results using the Q_{ref}^{*} obtained from the three control cases discussed in the previous subsection. In grid-connected PV systems, the inverter introduces harmonic currents, which are analyzed based on the Q_{ref}^{*} using (6)-(8). In this analysis, only the 5th and 7th harmonic orders were considered, as they have the most significant impact on harmonic current magnitudes. The corresponding α_h in (8) were set to 5.05% for the 5th harmonic and 2.59% for the 7th harmonic [11]. These results are then used to calculate the harmonic voltages and voltage THD using (9)-(10). Fig. 6 illustrates the 24-hour variation of the 5th and 7th harmonic voltage magnitudes, as well as the THD of voltage, under three control modes.

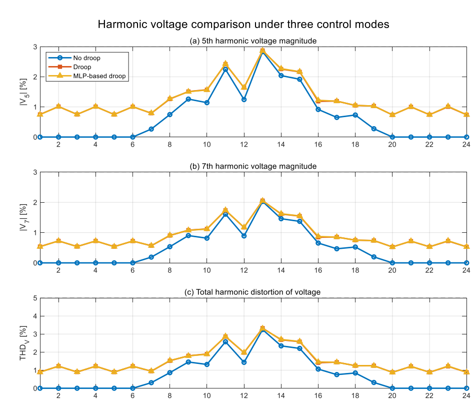

Fig. 6. Harmonic voltage comparison under three control modes: (a) 5th harmonic voltage, (b) 7th harmonic voltage, and (c) THD of voltage.

979-8-3315-8138-1

As shown in Fig. 6, when the Volt/Var droop control is not applied, harmonic voltages appear only during PV generation period (from 06:00 to 20:00), while they remain zero outside this period due to the absence of inverter operation. Around 13:00, although the Q_{ref}^* reaches its minimum, the harmonic voltage exhibits the highest magnitude because the PV generation is at its peak. Moreover, the predicted harmonic voltages from the MLP-based control closely match those of the conventional droop control while satisfying the IEEE 519 standard. Therefore, it can be concluded that the proposed MLP-based Volt/Var control provides accurate harmonic voltage prediction and maintains consistent harmonic performance.

IV. Discussion

This study compared the Q_{ref}^* generated by three methods (i.e., conventional droop control, the proposed MLP-based model, and the regression model). The MLP-predicted Q_{ref}^* exhibited behavior that was nearly identical to the conventional droop output. This outcome indicates that the MLP effectively acquired the nonlinear droop characteristics. The regression model exhibited a similar trend, although with slightly greater deviations, particularly at the first time step. This is due to its simplified polynomial structure. Quantitatively, the regression model showed an RMSE of 3.34×10^{-2}, an MAE of 2.34×10^{-2}, and a maximum deviation of 0.109 p.u. when evaluated against the conventional droop output. Despite these differences, both the MLP and regression-based Q_{ref}^* produced voltage profiles consistent with those of the conventional method. Furthermore, the harmonic voltage and THD results remained closely aligned across three approaches (without droop, conventional droop method, and MLP-based method). These findings demonstrate that the MLP-based Volt/Var control method preserves the performance of traditional droop control while enabling fast, non-iterative computation suitable for real-time operation, with the regression model serving as an additional lightweight surrogate. Future work will extend the framework to adaptive droop parameter tuning and N-1 contingency scenarios.

V. Conclusion

This paper proposed an MLP-based Volt/Var control method designed to improve the voltage regulation capability of PV inverters under time-varying load and generation conditions. The MLP model was trained using 57,600 samples generated from dynamic droop scenarios and demonstrated strong regression performance with a R of 0.997. In the case study presented in Section B, the proposed MLP-based control exhibited almost identical Q_{ref}* tracking to the conventional droop method, with a minimum validation MSE of 5.97×10^{-4} during training. When applied to power flow simulations, the MLP-based control achieved highly accurate voltage regulation, showing an MSE of 7.27×10^{-7}, a MAE of 5.14×10^{-4}, and a maximum deviation of only 0.0025p.u. compared with the conventional droop method. Furthermore, harmonic analysis based on the predicted Q_{ref}^* confirmed that the MLP-based approach maintained the same harmonic voltage and THD trends as the conventional droop. These results demonstrate that the proposed MLP-based Volt/Var control maintains comparable performance to the conventional method while offering superior adaptability and prediction accuracy under uncertain grid conditions. Future work will focus on extending the model to dynamically adjust droop parameters in real time and to enhance robustness through the investigation and application of various AI models. In addition, future research will develop a regression model capable of estimating the harmonic impacts caused by the Q^*, enabling a more comprehensive assessment of power quality.

VI. Appendix A

The identified coefficients of the surrogate regression model described in (11) are summarized in Table A.1.

Table A.1. Identified coefficients a_i and b_i (for i = 1, 2, …, 13)

Component	Values
a_i	-230.37, -0.317, 1.151, 0.378, 0.207, 0.013, 20.17, 12.95, 82.19, 4.13, -0.233, -0.997, -0.367
b_i	112.04, 0.350, -1.842, -0.199, -0.099, -0.0014, -10.22, -4.95, -37.03, -1.92, 0.13, 0.621, 0.529
c_0	52.48

References

[1] O. Gandhi, D. S. Kumar, C. D. Rodríguez-Gallegos, and D. Srinivasan, "Review of power system impacts at high PV penetration Part I: Factors limiting PV penetration," *Solar Energy,* vol. 210, pp. 181-201, 2020/11/01/ 2020, doi: https://doi.org/10.1016/j.solener.2020.06.097.

[2] M. Karimi, H. Mokhlis, K. Naidu, S. Uddin, and A. H. A. Bakar, "Photovoltaic penetration issues and impacts in distribution network – A review," *Renewable and Sustainable Energy Reviews,* vol. 53, pp. 594-605, 2016/01/01/ 2016, doi: https://doi.org/10.1016/j.rser.2015.08.042.

[3] K. R. Babu and D. K. Khatod, "Smart Inverter-Based Distributed Volt/Var Control for Voltage Violation Mitigation of Unbalanced Distribution Networks," *IEEE Transactions on Power Delivery,* vol. 39, no. 3, pp. 1481-1490, 2024, doi: 10.1109/TPWRD.2024.3372603.

[4] P. Jahangiri and D. C. Aliprantis, "Distributed Volt/VAr control by PV inverters," *IEEE Transactions on power systems,* vol. 28, no. 3, pp. 3429-3439, 2013.

[5] T. Bashir, H. Wang, M. Tahir, and Y. Zhang, "Wind and solar power forecasting based on hybrid CNN-ABiLSTM, CNN-transformer-MLP models," *Renewable Energy,* vol. 239, p. 122055, 2025/02/01/ 2025, doi: https://doi.org/10.1016/j.renene.2024.122055.

[6] J. P. Carmichael and Y. Liao, "Application of Deep Neural Networks to Distribution System State Estimation and Forecasting," (in English), *Frontiers in Sustainable Cities,* Original Research vol. Volume 3 - 2021, 2022-January-07 2022, doi: 10.3389/frsc.2021.814037.

[7] F. Kabir, N. Yu, Y. Gao, and W. Wang, "Deep reinforcement learning-based two-timescale Volt-VAR control with degradation-aware smart inverters in power distribution systems," *Applied Energy,* vol. 335, p. 120629, 2023/04/01/ 2023, doi: https://doi.org/10.1016/j.apenergy.2022.120629.

[8] S. Su *et al.*, "Volt-VAR Control in Active Distribution Networks Using Multi-Agent Reinforcement Learning," *Electronics,* vol. 13, no. 10, p. 1971, 2024. [Online]. Available: https://www.mdpi.com/2079-9292/13/10/1971.

[9] "IEEE Standard for Harmonic Control in Electric Power Systems," *IEEE Std 519-2022 (Revision of IEEE Std 519-2014),* pp. 1-31, 2022, doi: 10.1109/IEEESTD.2022.9848440.

[10] R. Christie. "UW Power System Test Case Archive." http://www.ee.washington.edu/research/pstca/ (accessed November 11, 2025.

[11] A. M. Enrique, M., *Power Systems Harmonics, Computer Modelling and Analysis*. New York, USA: John Wiley and Sons Inc., 2001.

979-8-3315-8138-1